Neurally-augmented immunity-based detection and identification of aircraft sub-system failures

M. G. Perhinschi
mario.perhinschi@mail.wvu.edu
West Virginia University, Morgantown
West Virginia, USA

H. Moncayo
Embry-Riddle Aeronautical University, Daytona Beach
Florida, USA

B. Wilburn, J. Wilburn, O. Karas and A. Bartlett
West Virginia University, Morgantown
West Virginia, USA

ABSTRACT

This paper presents the development and testing through simulation of an integrated scheme for aircraft sub-system failure detection and identification (FDI) based on the artificial immune system (AIS) paradigm augmented with artificial neural networks. The features that define the self within the AIS paradigm include neural estimates of the angular accelerations produced by the abnormal conditions. The simulation environment integrates the NASA Generic Transport Model interfaced with FlightGear. A hierarchical multi-self strategy was investigated for developing FDI schemes capable of handling malfunctions of a variety of aircraft sub-systems. The performance of the FDI scheme has been evaluated in terms of false alarms and successful detection and identification over a wide flight envelope and for several actuator and aerodynamic surface failures. For all cases considered, the performance was very good, confirming the potential of the AIS paradigm augmented with the proposed neural network-based approach for feature definition to offer a comprehensive solution to the aircraft sub-system FDI problem.

Paper No. 3963. Manuscript received 18 February 2013, revised version received 8 February 2014, accepted 6 March 2014.

https://doi.org/10.1017/S0001924000009532 Published online by Cambridge University Press

NOMENCLATURE

AIS	artificial immune system
ANN	artificial neural networks
$\hat{e}(k)$	neural estimation error
EMRAN	extended minimal resource allocation network
FDI	failure detection and identification
g	gravity
GTM	generic transport model
H	flight altitude
HMS	hierarchical multi-self
IFDOT	immunity-based failure detector optimisation and testing
k_{lat}, k_{lon}, k_{dir}	preliminary command scaling factors
K_p, K_i, K_d	proportional, integral, and derivative gains
n_{y_cmd}	preliminary lateral load factor command
n_{z_cmd}	preliminary vertical load factor command
NLDI	non-linear dynamic inversion
p_{cmd}	preliminary roll rate command
p_{com}, q_{com}, r_{com}	commanded angular rates
p_{ref}, q_{ref}, r_{ref}	reference model roll, pitch, and yaw rates
Thr_1	warning threshold
Thr_2	detection thresholds
U_p, U_q, U_r	pseudo-controls
$\bar{U}_p$, $\bar{U}_q$, $\bar{U}_r$	filtered pseudo-controls
UAV	unmanned aerial vehicles
V	aircraft velocity
w	neural weights
WVU	West Virginia University
x	neural network input vector
$\hat{y}$	neural output

Greek symbols

α	angle-of-attack
β	sideslip angle
$\delta_{lat_{stick}}$	lateral stick displacement
$\delta_{lon_{stick}}$	longitudinal stick displacement
$\delta_{dir_{pedal}}$	pedal displacement
η	neural learning rate
φ	roll attitude angle
μ	gaussian centre position
σ	gaussian variance
θ	set of neural network parameters
ζ	detection parameter

https://doi.org/10.1017/S0001924000009532 Published online by Cambridge University Press

1.0 INTRODUCTION

Aircraft operational safety has been consistently acknowledged within the aerospace engineering community as a major current priority[1-2]. The focus of numerous research efforts has been in recent years the development of methodologies for timely detection of upset/abnormal situations to ensure pilot situational awareness and trigger fault tolerant automatic compensation[3-6], while maintaining high levels of performance. Solving the problem of aircraft sub-system failure detection and identification (FDI) in a comprehensive manner is characterised by complexity and extremely high dimensionality. The integration of FDI schemes for a large diversity of aircraft sub-systems and over extended areas of the flight envelope poses significant challenges and requires adequate tools. A new concept inspired from the biological immune system was proposed for aerospace systems FDI[7,8]. The artificial immune system (AIS)-based fault detection operates in a manner similar to its biological counterpart — according to the principle of self-non-self discrimination — when it distinguishes between entities that belong to the organism (the self) and entities that do not (the non-self). Research at West Virginia University (WVU) in fault tolerant control laws has led to the development of an integrated computational framework[9,10] for aircraft sub-system FDI based on the AIS paradigm. Several classes of failures/damages affecting control actuators, sensors, propulsion system, and structural components over large areas of the flight envelope have been considered for a manned supersonic fighter[11,12] demonstrating that the AIS paradigm can address directly the complexity and multi-dimensionality of aircraft dynamic response in the context of abnormal conditions and provide the tools necessary for a comprehensive and integrated solution to the FDI problem.

The previously developed WVU AIS-based FDI schemes[11-13] relied on parameters computed within fault tolerant control laws augmented with artificial neural networks (ANN), which limits its application to aircraft equipped with such a control system. An alternative generalised solution is proposed in this paper by using *ad hoc* open-loop on-line training ANN, which are not aircraft dependent. The WVU integrated computational environment for design of aircraft sub-system FDI based on the AIS paradigm[14-16] is used to develop and test the alternative FDI scheme for an unmanned aerial vehicle (UAV). The current need of addressing flight upset conditions combined with the growing interest in UAV and their use as test platforms, led to the development by NASA of an advanced integrated testing system, the Airborne Subscale Transport Aircraft Research[17] (AirSTAR), which relies on remotely piloted subscale models. A high fidelity simulation model of the aircraft, the NASA Generic Transport Model[18] (GTM), has been made publicly available, was integrated with the WVU simulation environment, and used within this research effort.

The approach proposed in this paper by combining the function approximation and modeling capabilities of the artificial neural networks with the versatile potential for classification of multi-dimensional spaces possessed by the artificial immune system is expected to provide a flexible and widely applicable solution to the aircraft sub-system FDI problem.

The paper is organised as follows. The basics of the AIS paradigm are presented in Section 2.0. The general simulation environment used for development and testing is described in Section 3.0. The development of the AIS-based detection scheme and its main components, including the neural augmentation, are presented in detail in Section 4.0. The AIS detector generation and optimisation process is discussed in Section 5.0. The experiment design and data acquisition are presented in Section 6.0. Section 7.0 includes the discussion of the results and the evaluation of detection scheme performance. Finally, some conclusions are summarised in Section 8.0 followed by acknowledgements and a bibliographical list.

https://doi.org/10.1017/S0001924000009532 Published online by Cambridge University Press

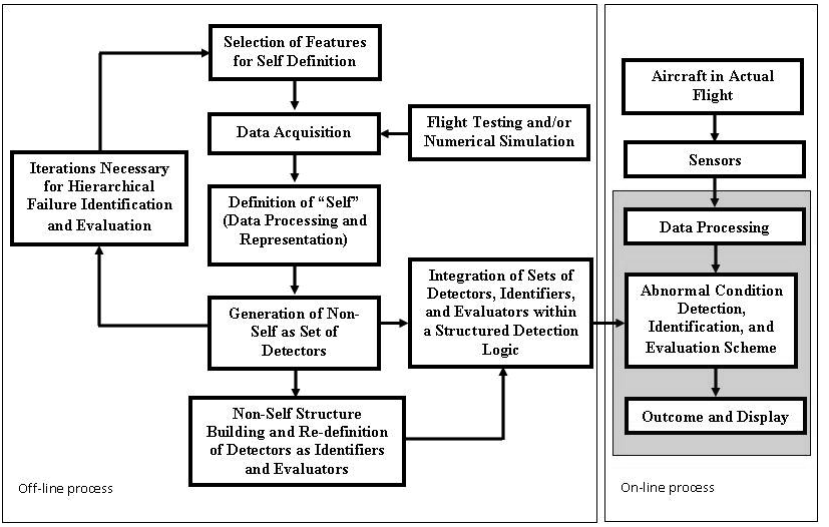


Figure 1. Artificial immune system-based abnormal condition detection, identification and evaluation.

2.0 THE ARTIFICIAL IMMUNE SYSTEM PARADIGM

In recent years, due to its robustness and adaptability, the biological immune system has been the inspiration for a new artificial intelligence technique, the artificial immune system. The biological immune system is responsible for distinguishing between the body's own cells and microbial and non-microbial exogenous entities, marking the intruders for destruction, and eventually destroying them with minimum energetic and toxic impact on the organism. This role is accomplished primarily through two major processes. One such process consists of the generation of specialised cells[19] (dendritic cells, T-cells, and B-cell) through a negative selection process which allows them to bind to biochemical markers that are specific to the antigen and not to the own organism. The other process is a regulatory process that controls the production of antibodies (the 'soldier' cells directly fighting the antigens) based on the nature and severity of the infection, the current balance between antibodies and antigens, and the perceived level of 'danger' and 'safety'.

The negative selection mechanism that produces antibodies whose chemical markers or features differ from those of the body's cells is the conceptual basis for the AIS for fault detection[20-22]. Under this paradigm, any configuration of 'features' that is not recognised as corresponding to nominal conditions, is considered to correspond to an abnormal condition. The set of 'features' used by the negative selection process may consist of any set of parameters that capture the signature of the abnormal condition. Examples of these features may include sensor measurements, system state estimations, pilot inputs, or statistical parameters relevant to system dynamic response. When constructing the 'self', or nominal portion of the hyper-dimensional variable space, large amounts of recorded data over extended areas of the flight envelope are needed. Due to computational and storage limitations, it is necessary to convert the data to a more manageable form. This is accomplished through duplicate elimination and data clustering, such that the self definition is represented as a collection of real-valued hyper-bodies. Similarly, the non-self is covered with hyper-bodies called detectors, the counterpart of the antibodies. The process of defining self and non-self may be repeated to generate different sets of detectors, capable of detecting different failures. These multiple non-selves may be combined in a hierarchical structure[11] to improve detection accuracy

https://doi.org/10.1017/S0001924000009532 Published online by Cambridge University Press

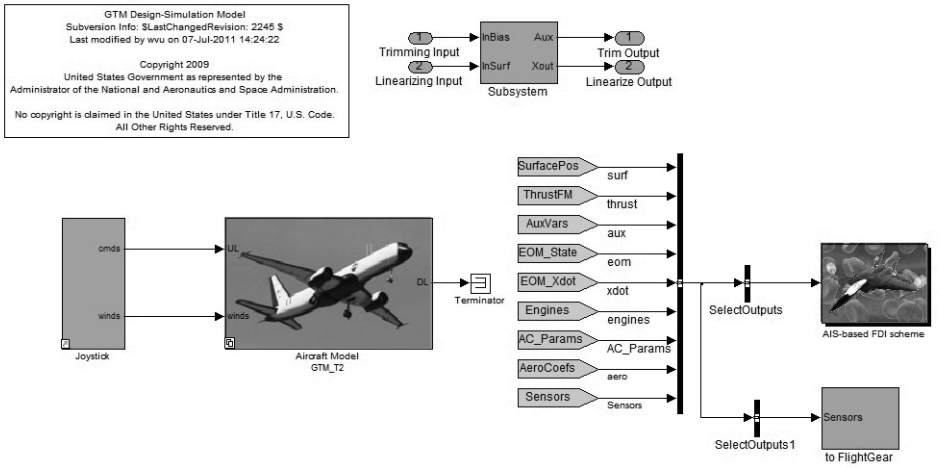


Figure 2. NASA GTM with FlightGear interface and AIS-based FDI scheme.

and computational efficiency. An integrated framework and extensive computational tools have been developed at WVU for the design of comprehensive detection schemes[23,24] for aircraft sub-system abnormal conditions. Structuring of the non-self hyper-space based on combined positive and negative selection mechanism allows for the extension of the detection schemes into failure identification and evaluation schemes. A block diagram illustrating the use of the AIS for abnormal condition detection, identification, and evaluation is presented in Fig. 1.

3.0 THE SIMULATION ENVIRONMENT

Tests to obtain the 'self' data were performed with an aircraft simulation model developed as part of NASA's Aviation Safety Program, which aims at enhancing aircraft safety technology in various areas such that a holistic solution is obtained to the problem of detecting, identifying, evaluating, and accommodating abnormal/upset flight conditions produced by a variety of factors as means of preventing and mitigating aircraft loss of control[25]. The NASA GTM[16], is a MATLAB/Simulink implementation of a remotely-controlled UAV representing a 5·5% geometrically and dynamically scaled-down Boeing 757 commercial airliner. It can be used to simulate extreme regions of the flight envelope, severe manoeuvres, upset flight conditions, and failures of several aircraft sub-systems. The model was integrated within the WVU UAV simulation environment[26,27] and was used to perform flight tests and collect data for developing and evaluating the performance of the WVU AIS-based FDI scheme over typical flight conditions. For visualisation purposes, the WVU UAV simulation environment uses FlightGear[28], an open-source highly flexible and versatile flight simulation software. A set of Simulink blocks were developed to accept and transfer joystick inputs to the GTM and send signals from the model to FlightGear for visualisation, as shown in Fig. 2. A view of the pilot visual interface provided by FlightGear is presented in Fig. 3.

For the purpose of this paper, the development of the FDI scheme using the WVU evolutionary algorithm-based tools[14] as well as the simulation tests with the GTM were performed on a computer with specifications listed in Table 1.

https://doi.org/10.1017/S0001924000009532 Published online by Cambridge University Press



Figure 3. FlightGear interface driven by NASA GTM within WVU UAV simulation environment.

A set of failure scenarios have been considered for testing and evaluating the performance of the proposed FDI scheme as outlined in Table 2. It should be noted that, due to the symmetry of the aircraft, the dynamic fingerprint of these types of failures and damages occurring on the left side are similar to those occurring on the right side. Some of these scenarios were available within the GTM model (first six failures outlined in Table 2). Additional customisation of the model was performed to implement more types of failures, such as jam of elevator and aileron control surfaces at 5deg (last four failures outlined in Table 2).

Table 1
Hardware and software main characteristics

System	Microsoft Windows XP, Professional x64 Edition, Version 2003, Service Pack 2
Computer	Intel (R) Core (TM) i7 CPU 975 @ 3.33GHz, 3.34 GHZ, 11.9 GB of RAM
MATLAB	Version: 7.9.0.529 (R2009b), 64-bit (win64)
Simulink	Version: 7.5 (R2010a)
FlightGear	Version: 2.0.0

https://doi.org/10.1017/S0001924000009532 Published online by Cambridge University Press

Table 2
Simulated failures

Failure type	Description
Rudder off	Entire rudder missing. Complete loss of rudder control power — all control moments due to rudder deflection are cancelled.
Vertical tail off	Entire vertical tail is missing affecting directional stability and including complete loss of rudder control power.
Left outboard flap off	Left outboard trailing edge flap is missing. A rolling moment bias is generating and the left wing rolls downward. Roll control is required to compensate for roll asymmetry, thus available roll control power is reduced.
Left wingtip off	The outboard left wing tip including left aileron (approx 25% semi-span) is missing. All effects due to left aileron deflection are cancelled.
Left elevator off	The entire left elevator is lost. The pitch control power is reduced. All effects due to left elevator deflection are cancelled. Remaining pitch control activity (right elevator) will generate rolling moments due to control asymmetry.
Left stabiliser off	The entire left stabiliser is lost. The same dynamic effects occur as for the left elevator missing case with an increase in the rolling moment due to the more severe lift asymmetry.
Left elevator jam	The left longitudinal control surface is locked at 5˚.
Right elevator jam	The right longitudinal control surface is locked at 5˚.
Left aileron jam	The left lateral control surface is locked at 5˚.
Right aileron jam	The right lateral control surface is locked at 5˚.

4.0 AIRCRAFT SUB-SYSTEM FAILURE DETECTION AND IDENTIFICATION SCHEME

The AIS scheme for FDI is based on a hierarchical multi-self (HMS) strategy[11], which relies on the assumption that a specific set of parameters could favor the detection of some particular failures better than others. This approach requires building failure specific 'selves' and identification of low dimension spaces for hierarchical 'selves' definitions. With this configuration, the AIS-based FDI scheme, as an integrated system, is capable of detecting and identifying a large variety of upset conditions of all main aircraft sub-systems over a wide range of severity while avoiding the use of one large dimensional 'self' for centralised detection and/or identification, which typically requires a more substantial computational effort and is exposed to numerical issues. As shown in Fig. 4, the online failure detection, identification, and evaluation processes are performed in subsequent phases using three main components. The first one uses an integrated block of self patterns, which performs the detection phase. The second component, where the identification phase is performed, attempts to ensure the correct identification of categories and sub-categories of failures at different levels. The third component performs a qualitative and quantitative evaluation of the failure. At this point, the magnitude or severity of the failure is determined as well as the impact of the detected failure on the flight envelope of the aircraft. This last evaluation feature is not implemented for the purposes of this paper.

https://doi.org/10.1017/S0001924000009532 Published online by Cambridge University Press

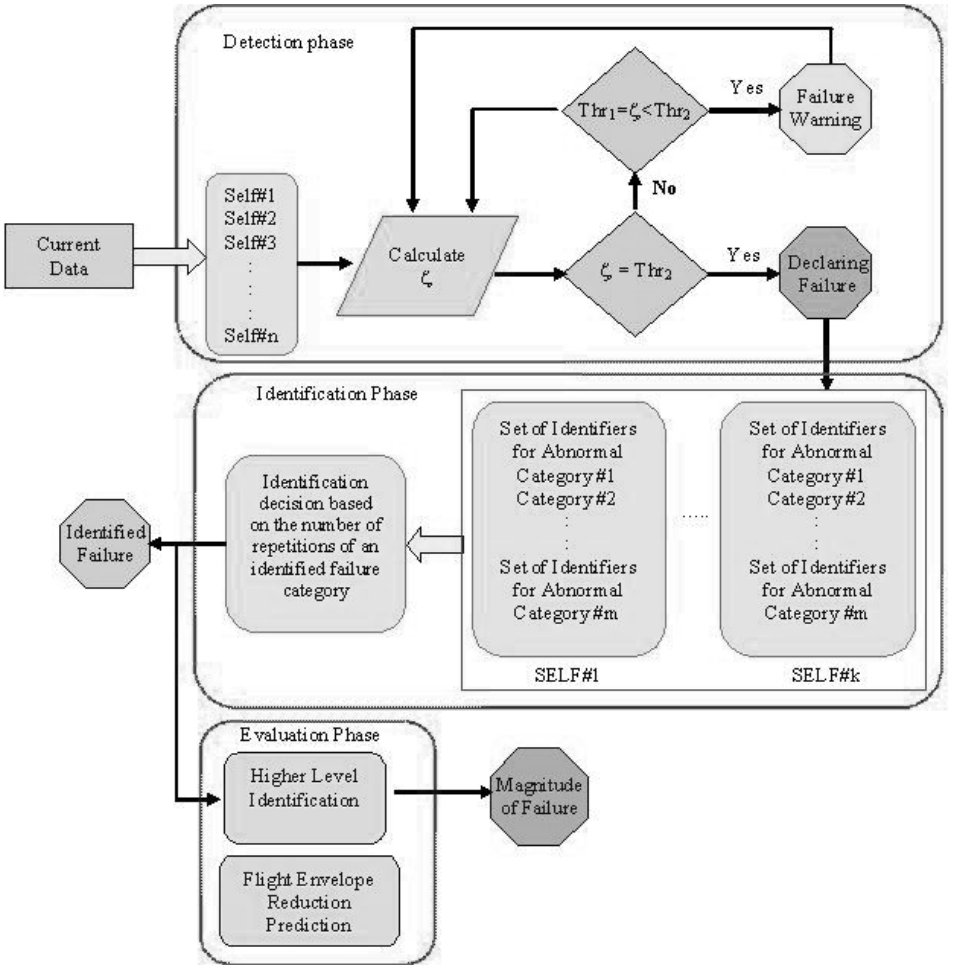


Figure 4. Logic block diagram for on-line failure detection, identification and evaluation.

Figure 2 shows the highest level of a generic AIS-FDI Simulink scheme integrated with the GTM simulation package. At this level, features obtained through simulation (measured in flight in a real situation) are provided to the AIS to be monitored by the antibodies. With this scheme, the capabilities of the system to detect the failures considered can be studied on-line. The output of the scheme consists also of a message display to warn the pilot regarding the failure.

4.1 Detection

Detection represents the process of declaring that a generic malfunction of the system has occurred. Any one or several of the sub-systems can be subject to the failure. These sub-systems can be actuators, sensors, propulsion, structural elements, etc. During this phase, using an integrated block of self patterns, sets of current values of the features measured in flight at a certain sampling rate are compared against the detectors that have been generated for every self configuration, through negative selection, as shown in Fig. 4. A detection parameter ζ is calculated, which represents the number of consecutive points over a time window that trigger detectors, summed over all selves.

https://doi.org/10.1017/S0001924000009532 Published online by Cambridge University Press

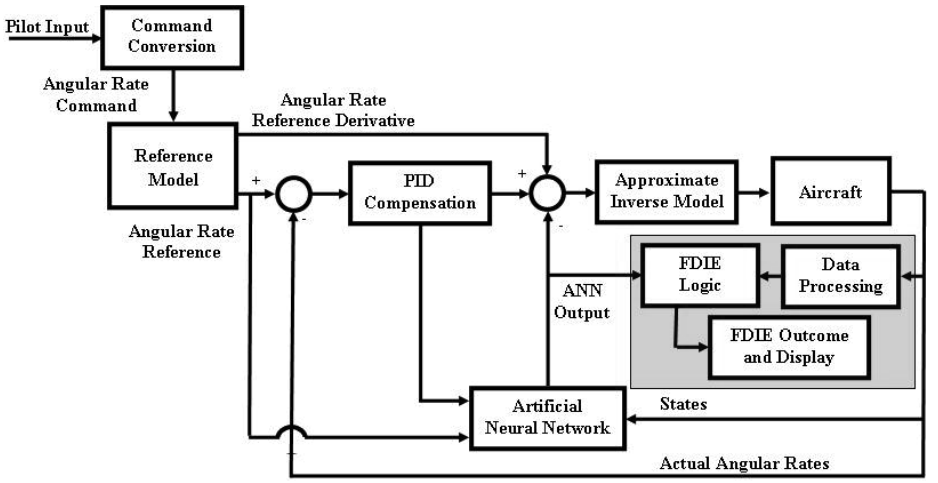


Figure 5. General block diagram of the FDIE scheme and NLDI+ANN control laws.

If ζ is within a certain range, a failure warning is issued, but if ζ exceeds the upper bound of the range, a failure is declared and the identification phase starts.

4.2 Identification

The identification process of the AIS-based FDI scheme consists of determining in which of the categories the failure falls or, in other words, determining what is the failed subsystem and/or what is the type of failure. For instance, the failure could be attributed to one of the ten categories outlined in Table 2. The different hierarchical selves can be associated through feature selection and design to specific failure categories. Within each self, the detectors are labeled to correspond to specific failures through a positive-selection-type of mechanism, thus becoming 'identifiers'. Note that some of these sets may be empty if the particular self does not capture the signature of certain failures. As shown in Fig. 4, the category is determined based on the number of times each set of identifiers is activated over a time window for all selves. The identified failure category is the one corresponding to the set of identifiers that is activated more often.

4.3 Selection of features for self definition

The selection of the appropriate parameters to build the 'self' of nominal conditions is a critical step for the success of the AIS-based FDI scheme. Previous research efforts at WVU[9-12,23], have shown that the following five categories of parameters could be used in general for self/non-self definition: aircraft state variables, pilot input variables, stability and control derivatives, variables generated within the control laws, and derived variables. They can be instantaneous samples or time histories over constant or variable time windows.

Particular interest has generated the use of parameters computed within the control laws since they have been determined to possess very good detection capabilities[9,13,23]. Specifically, direct adaptive control laws with a 'model following' architecture based on non-linear dynamic inversion (NLDI) augmented with ANN were considered. The block diagram of this configuration integrating the FDI with the fault tolerant control laws is presented in Fig. 5.

https://doi.org/10.1017/S0001924000009532 Published online by Cambridge University Press

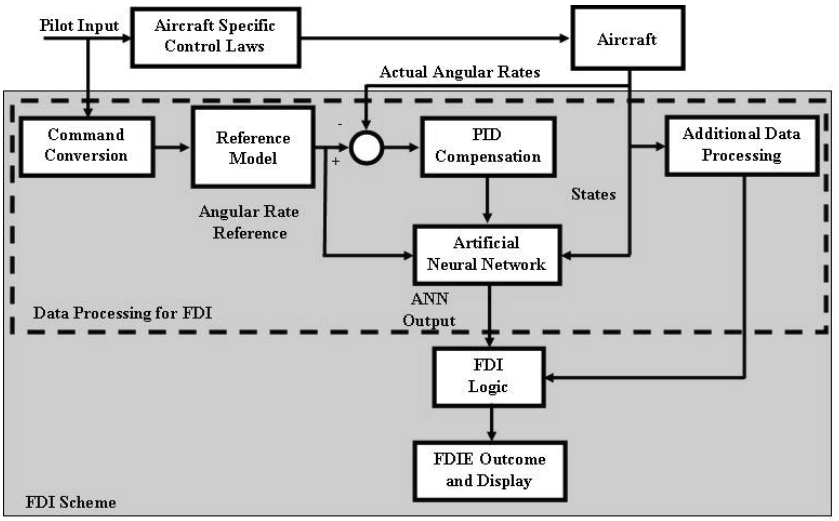


Figure 6. General block diagram of the FDI scheme augmented with ANN.

Note that the ANN operate 'closed-loop', thus in order to utilise the FDI scheme, the aircraft must be equipped with such a specific control system. To avoid this limitation, a new architecture for the FDI scheme is investigated in this paper, in which the ANN are included as part of the data processing block (see Fig. 6). The ANN operate now 'open-loop' and are no longer part of the control laws. The approach ensures portability of the FDI scheme to various platforms irrespective of their control systems. The potential of the ANN outputs for self definition and capturing the dynamic fingerprint of a variety of actuator and structural failures are analysed in this paper.

The ANN outputs represent estimates of the angular accelerations on the three body axes (roll, pitch, and yaw) produced by the off-nominal conditions. These parameters together with the body axes angular rates have been considered in this paper to define the self within the AIS paradigm based on previous analyses[9,13].

4.4 ANN outputs for self definition

The pilot inputs in terms of stick and pedal displacements ($\delta_{lat_{stick}}$, $\delta_{lon_{stick}}$, $\delta_{dir_{pedal}}$) are first converted into preliminary commanded aircraft states (roll rate p_{cmd}, vertical load factor n_{z_cmd}, and lateral load factor n_{y_cmd}) through scaling:

$$\begin{aligned} p_{cmd} &= k_{lat}\delta_{lat_{stick}} \\ n_{z_cmd} &= k_{lon}\delta_{lon_{stick}} \\ n_{y_cmd} &= k_{dir}\delta_{dir_{pedal}} \end{aligned} \quad \ldots (1)$$

The commanded angular rates (p_{com}, q_{com}, r_{com}) are then obtained as:

$$\begin{aligned} p_{com} &= p_{cmd} \\ q_{com} &= \frac{g}{V} n_{z_cmd} \\ r_{com} &= \frac{g}{V}(n_{y_cmd} + \mathrm{Sin}(\phi)) \end{aligned} \quad \ldots (2)$$

https://doi.org/10.1017/S0001924000009532 Published online by Cambridge University Press

where g is gravity, V is velocity and φ is the roll attitude angle.

First order roll rate and second order pitch and yaw rate reference models are used to determine the desired aircraft response in terms of reference angular rates (p_{ref}, q_{ref}, r_{ref}):

$$\begin{aligned} p_{ref}(s) &= \frac{1}{\tau_{roll}s+1}p_{com}(s) \\ q_{ref}(s) &= \frac{\omega_{pitch}^2}{s^2+2\varsigma_{pitch}\omega_{pitch}+\omega_{pitch}^2}q_{com}(s) \\ r_{ref}(s) &= \frac{\omega_{yaw}^2}{s^2+2\varsigma_{yaw}\omega_{yaw}+\omega_{yaw}^2}r_{com}(s) \end{aligned} \quad \ldots (3)$$

Tracking errors are computed as the difference between desired and actual angular rates:

$$e_\omega = \omega_{ref} - \omega \quad \ldots (4)$$

where ω represents p, q or r. These tracking errors are used to provide proportional, integral, and derivative compensation within the fault tolerant control laws. Here, for FDI purposes, the pseudo-controls in terms of angular acceleration commands (U_p, U_q, U_r) are only used as inputs to the ANN. These parameters are evaluated using:

$$U_\omega = \left(K_{p_\omega} + \frac{K_{i_\omega}}{s} + K_{d_\omega}s\right).e_\omega + s.\omega_{ref} \quad \ldots (5)$$

where K_p, K_i, and K_d are the constants of a proportional-integral-derivative type controller, respectively. Note that these parameters, as well as the reference models considered earlier, can be generic since the output of the ANN is not used for control purposes. It is the difference between this output at normal and abnormal conditions that is used for FDI.

An improved radial basis function ANN has been implemented for the purpose of this paper: the extended minimal resource allocation network[29] (EMRAN). The EMRAN is an on-line learning feedback network. It features a growing and pruning mechanism allowing the allocation of additional neurons in regions of the state space where the mapping accuracy is poor while avoiding the excessive growth of the network. Only the parameters of the most activated neurons are updated; therefore, the computational effort is minimised for this class of neural augmentation. For Gaussian basis functions, the estimate is computed as a weighted sum over all N neurons, with the expression:

$$\hat{y}(x,\theta) = \sum_{i=1}^{N} w_i e^{\left(\frac{|x-\mu_i|^2}{2\sigma_i^2}\right)} \quad \ldots (6)$$

where x is the input vector, θ is the set of parameters to be tuned by the learning algorithm including the weights w, the Gaussian centre positions μ, and the variances σ. A new neuron is initiated if three distinct criteria are simultaneously satisfied: the estimation error, the windowed estimation error, and the distance from the input to the nearest centre must each be larger than selected thresholds. If one of the criteria is not met, the tuning parameters are updated using the relationship:

$$\theta(k+1) = \theta(k) - \eta \left.\frac{\partial \hat{y}(k)}{\partial \theta(k)}\right|_{(k)} \cdot \hat{e}(k) \quad \ldots (7)$$

https://doi.org/10.1017/S0001924000009532 Published online by Cambridge University Press

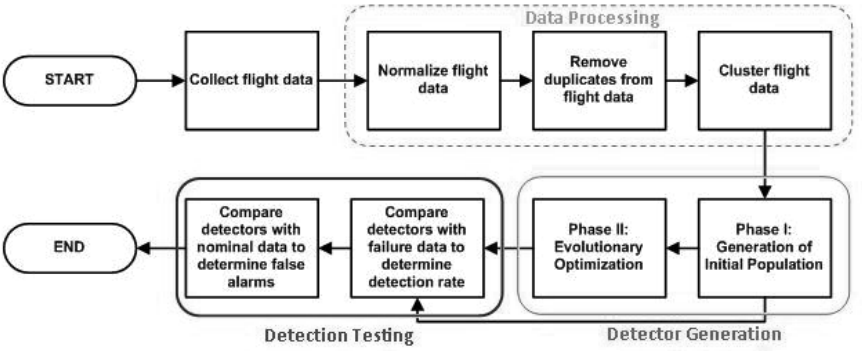


Figure 7. Flowchart of IFDOT utility processes.

where $\hat{e}(k)$ is the estimation error and η is the learning rate. The estimation error is assumed to be:

$$\hat{e}_{\omega} = \left(\hat{K}_{p_{\omega}} + \frac{\hat{K}_{i_{\omega}}}{s} \right) . e_{\omega} \quad \ldots (8)$$

The input to the ANN is:

$$x = \left[V \; H \; \alpha \; \beta \; \omega \; \omega_{ref} \; \bar{U}_{\omega} \right]^{T} \quad \ldots (9)$$

where V is the aircraft velocity, H is the altitude, α is the angle-of-attack, and β is the sideslip angle. These four inputs are the same on all three channels. For the longitudinal channel, $\omega = q$, while for the lateral and directional channels, $\omega = [p \; r]$. Only on-channel variables are considered for ω_{ref} and $\bar{U}_{\omega}$. Finally, $\bar{U}_{\omega}$ is defined as:

$$\bar{U}_{\omega} = \frac{1 - e^{(\hat{y} - U_{\omega})}}{1 + e^{(\hat{y} - U_{\omega})}} \quad \ldots (10)$$

where $\hat{y}$ is the previous output of the ANN.

5.0 GENERATION AND OPTIMISATION OF AIS DETECTORS

Extensive experimental data are necessary to determine the 'self' or the hyper-space of normal conditions. Adequate numerical representations of the self/non-self must be used and the data processed such that they are manageable given the computational and storage limitations of the available hardware. A set of integrated tools referred to as the WVU immunity-based failure detector optimisation and testing (IFDOT) environment has been developed[13,14,24] for the purpose of processing data to create the self, generating and optimising immunity-based detectors for use in various detection logics, and testing of individual sets of detectors to determine detection performance. A general flowchart of the processes carried out by this utility is shown below in Fig. 7. The main menu for this utility is presented in Fig. 8. The following sections contain an overview of the algorithms implemented in the IFDOT utility.

https://doi.org/10.1017/S0001924000009532 Published online by Cambridge University Press

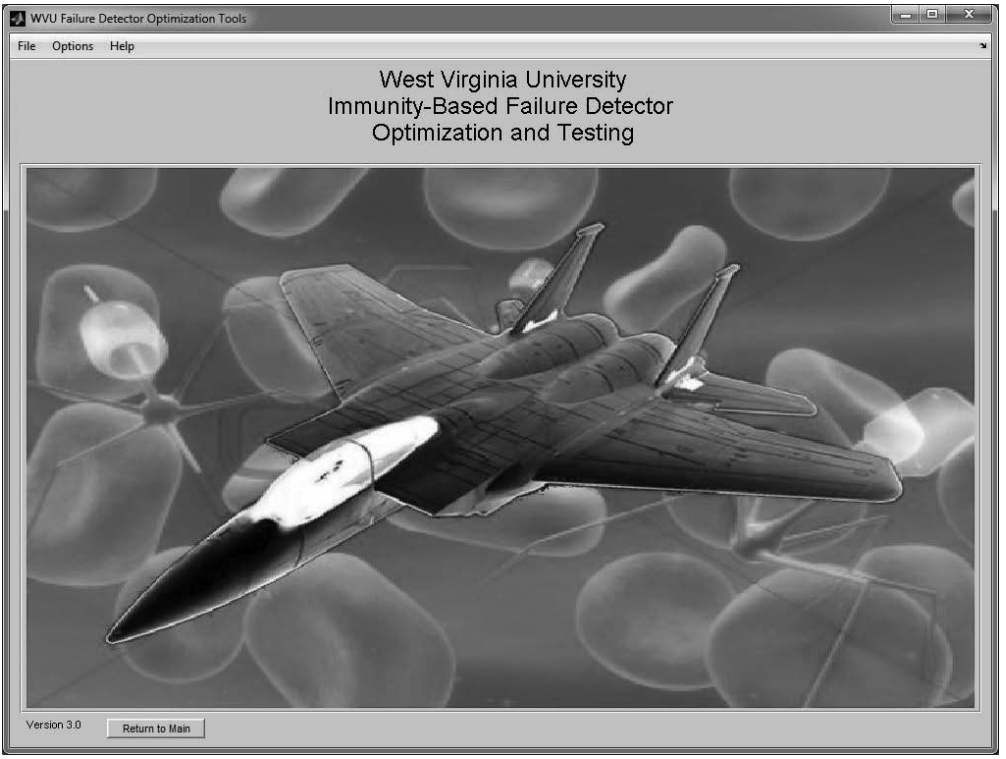


Figure 8. Main menu of the WVU AIS design environment[24].

5.1 Data representation

Prior to the generation of detectors, or antibodies, for AIS-based FDI, a set of variables/features must be defined which are expected to be capable of capturing the fingerprint of the various failures for which the antibodies are designed. For a complete and accurate description of the self, or the hyper-space of normal conditions, adequate coverage of the solution space must also be achieved. Thus, large amounts of data are typically needed to define the self. The self/non-self consists of sets of n-dimensional points representing all combinations of selected n variables (features). For aircraft sub-system fault detection, these sets of points are the collection of all time histories over, ideally, the entire flight envelope. However, to reduce the computational effort, both the self and the non-self are represented as sets of hyper-spheres through clustering.

5.2 Data processing

Substantial data processing is necessary to reduce the amount of data, and thus the computational workload. Normal condition data used to define the self undergo three stages of preprocessing: normalisation, removal of duplicates, and clustering. The data vector representing each feature is normalised from 0 to 1. Then, each data point in the solution space is compared with the other points to determine similarity. If a point is too similar to another point (i.e. the distance between the points is below a threshold), the points are considered identical and one is removed from the data set. Finally, the data are clustered using an enhanced k-means algorithm[23]. This process reduces the data from representation as individual points to representation as geometric hyper-bodies

https://doi.org/10.1017/S0001924000009532 Published online by Cambridge University Press

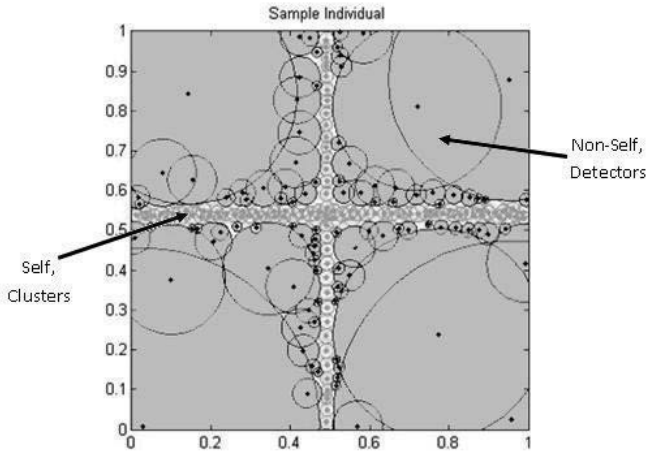


Figure 9. Two-dimensional example of an individual using hyper-spheres.

or clusters. In the case of the GTM, only hyper-sphere clusters were utilised. It should be noted that clustering necessarily introduces some 'empty space', or area of the solution space which is considered to be self, but which may actually be either self or non-self. Clustering data using a small number of clusters produces larger clusters, which may contain a large amount of empty space. This can lead to a reduction in detection performance. However, clustering with a large number of clusters, while reducing empty space, can potentially exclude areas of the variable space which should actually be classified as self, leading to an increased number of false alarms. Thus, this parameter should be chosen with care in order to obtain a good self definition. An enhanced clustering algorithm may be utilised, which will attempt to minimise empty space within clusters to within a specified tolerance. This is done by clustering the data using an increasing number of centres, until the clusters are within the allowable empty space threshold[23].

5.3 Detector generation and optimisation

Generation and optimisation of detectors is performed by two sets of algorithms. During Phase I, detectors are randomly generated through one of two methods. A negative selection algorithm is utilised to cover the non-self regions of the feature space with detectors to a desired coverage threshold, without allowing overlapping with the self clusters. This algorithm makes use of variable detector radii. Centres are generated at random within the feature space. Those that do not fall within another detector or the self have a radius set, which is equal to the shortest distance from the candidate centre to the nearest self cluster. This process ceases when enough detectors have been generated or the desired coverage is met.

An enhanced method[23] for detector generation attempts to minimise overlapping among detectors. This method functions in much the same way as the previous; however, it implements moving of unacceptable centres and cloning of matured detectors in order to achieve detectors with an acceptable amount of overlapping among the non-self. Only detectors passing this threshold are matured into the final set. A decay parameter is used to define when a candidate centre has been moved too many times and needs to be discarded. As in the previous detector generation method, no overlapping is permitted with the self region of the solution space. An example set of two-dimensional detectors can be seen in Fig. 9.

https://doi.org/10.1017/S0001924000009532 Published online by Cambridge University Press

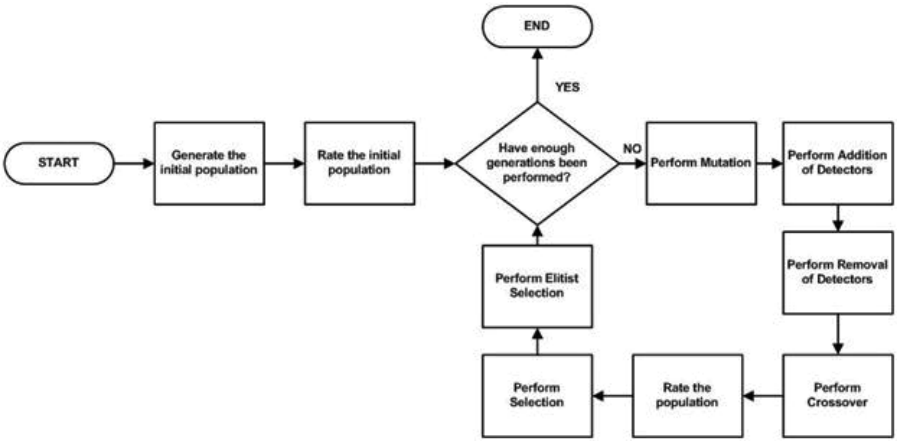


Figure 10. Flowchart of genetic algorithm for AIS detector generation and optimisation.

Once generated, detectors can be immediately used in a detection scheme. However, detectors generated in this way also form the starting point for Phase II, detector optimisation. In Phase II, a classic genetic algorithm is utilised to optimise the detectors for increased coverage of the non-self space, reduced overlapping among detectors, and reduced number of detectors in the set. In this algorithm, an individual is a set of detectors, while the population is composed of many sets of detectors. For example, the set of detectors presented in Fig. 9 form an individual (a potential solution to the problem). The genetic algorithm implements the roulette wheel selection strategy and elitist selection. It terminates after a prescribed number of generations. A flowchart of this algorithm is presented in Fig. 10. Four customised genetic operators were designed and implemented: mutation, crossover, addition, and subtraction. Mutation is intended to produce small alterations to existing detectors by randomly producing small changes in the parameters of a single detector within an individual. Crossover is intended to exploit good traits within existing individuals by trading a few detectors between two randomly selected individuals. Addition is intended to increase coverage of the non-self space without increasing overlap among detectors by adding a number of new detectors to a randomly selected individual, which overlap no other object. Subtraction is intended to decrease the amount of overlapping within a detector set by removing one or more of the detectors exhibiting the most overlap from a randomly chosen individual. This genetic operator should be used sparingly, as removal of detectors may uncover areas in the non-self region that were previously covered, decreasing the performance of the detector set[24].

5.4 Detector generation and optimisation for GTM

Detector generation for the GTM model takes place utilising the methods defined above. The proposed approach is demonstrated by selecting as self-defining features the angular rate components in body axes (p, q and r) and the ANN-based estimates of angular accelerations (*NNp*, *NNq*, and *NNr*) required to achieve desirable aircraft response, as outlined in Section IV. These features were grouped in three different 'selves' as presented in Table 3 to demonstrate the HMS strategy. Note that Self 1 and 2 are three-dimensional, while Self 3 is six-dimensional. The features used for Self 3 are the union of the sets used for the other two selves. Selves 1 and 2 can be regarded as lower order projections of self 3.

https://doi.org/10.1017/S0001924000009532 Published online by Cambridge University Press

Table 3
Feature configurations for self definition

Self number	Features	Feature space dimension	Number of antibodies
Self 1	*p*, *q*, *r*	3	643
Self 2	*NNp*, *NNq*, *NNr*	3	529
Self 3	*p*, *q*, *r*, *NNp*, *NNq*, *NNr*	6	735

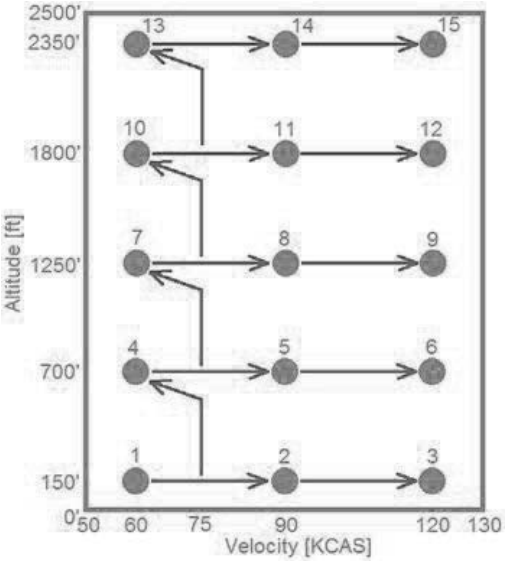


Figure 11. GTM flight envelope showing test points and transitions.

The selves are generated from extensive flight simulation data using hyper-sphere clusters for the GTM normal condition definition. Hyper-sphere detectors are produced, utilising the Phase I enhanced negative selection algorithm with variable detector radius[23] (ENSA-RV). Optimisation through the Phase II genetic algorithm is not performed in this study. Thus, the optimisation techniques defined above for the ENSA-RV algorithm are relied upon to produce adequate coverage of the solution space, and ensure no overlapping with the self and less than the specified maximum overlapping among the non-self.

6.0 EXPERIMENT DESIGN AND DATA ACQUISITION

The GTM was flown manually with a joystick-throttle configuration through various strategic points distributed across the whole flight envelope defined by the minimum and maximum flight altitude and velocity limits of the aircraft. Uniformly distributed points within the envelope were determined as shown in Fig. 11. The GTM dynamic aircraft model was then flown at the speeds and altitudes prescribed for each point. Manoeuvres were performed to excite the aircraft dynamics in all three axes. Roll doublets were performed first, followed by pitch doublets and yaw doublets. A climbing turn in one direction was then executed with an altitude gain of about 100ft. Finally, a

https://doi.org/10.1017/S0001924000009532 Published online by Cambridge University Press

Table 4
Detection performance summary

	Detection rates [%]				
Failure type	**Detection scheme #1 (Self #1)**	**Detection scheme #2 (Self #2)**	**Detection scheme #3 (Self #3)**	**Detection scheme #4 (Self #1 and #2)**	**Detection scheme #5 (Self #1, #2, #3)**
Rudder off	0·00	95·53	38·88	95·53	95·52
Vertical tail off	93·88	95·25	96·20	96·42	96·42
Left outboard flap off	42·50	95·40	99·43	98·52	99·58
Left wingtip off	31·73	98·20	97·85	98·95	99·03
Left elevator off	6·25	95·85	94·15	95·87	97·20
Left stabiliser off	60·00	45·20	91·40	96·80	98·85
Left elevator jam	11·14	89·41	95·60	93·23	99·20
Right elevator jam	4·37	89·78	95·68	92·18	98·33
Left aileron jam	10·77	66·89	97·78	90·32	98·37
Right aileron jam	18·34	87·38	98·80	92·30	98·80
Average	28	86	91	95	98

descending turn in the opposite direction was carried out. The aircraft was then accelerated to the next point in the flight envelope. Once 120kt calibrated airspeed (KCAS) was reached, a climb at a constant airspeed of 75 KCAS was established in order to reach the following target altitude. Just before reaching the target altitude, the aircraft was slowed to 60 KCAS and manoeuvers were resumed once the prescribed point in the flight envelope was reached. Figure 11 shows the location of the test points, at which the manoeuvres were carried out, as well as transitions that allow the aircraft to reach the following point. One flight test over the course of approximately one hour is necessary to cover the whole flight envelope at each failure or nominal condition. The tests were split in segments of approximately 10-15 minutes. The flight scenarios were first simulated under normal flight conditions. Then, they were repeated under various failure scenarios. Only one failure at a time is considered to capture/isolate the dynamic fingerprint of each type of failure. Separate sets of data were collected and used for development and validation.

7.0 EVALUATION OF THE FDI SCHEME

Five different detection schemes were developed based on the three individual selves, self #1 and #2, and all three selves together. Note that each of the first three schemes uses one single self outcome. The fourth scheme uses two outcomes and the fifth scheme, three outcomes. Their individual capability of capturing the fingerprint of the ten different abnormal conditions was evaluated in terms of detection rates and false alarms. The detection rate was computed as the percentage of all data samples that triggered a detector for the entire data set in the presence of the respective failures. The false alarm rate was computed as the percentage of all data samples that triggered a detector for the entire data set at nominal conditions. Note that the evaluation data set was a different set of data than the one used to build the self (or train the AIS).

The detection results over the entire test data are summarised in Table 4. An average of the detection rate over all failures considered is also included to facilitate comparison. For all schemes

https://doi.org/10.1017/S0001924000009532 Published online by Cambridge University Press

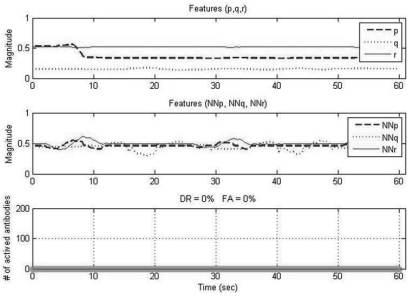


Figure 12. Nominal condition case.

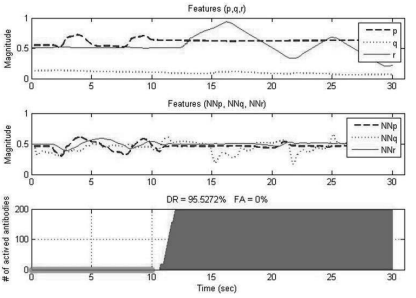


Figure 13. Rudder off case.

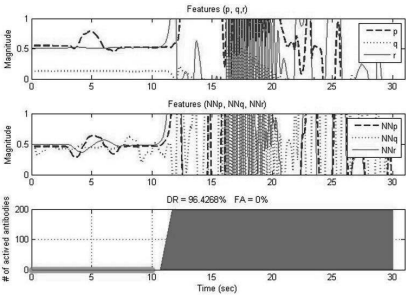


Figure 14. Vertical tail off case.

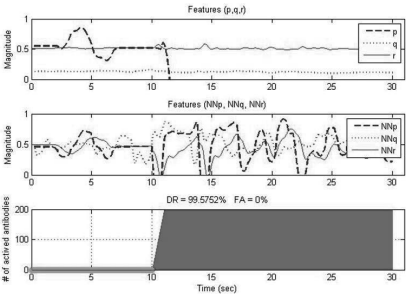


Figure 15. Left outboard flap off case.

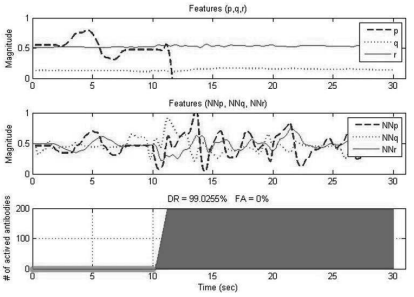


Figure 16. Left wingtip-off case.

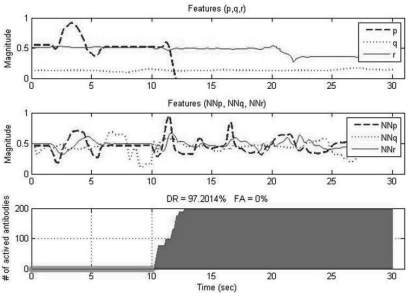


Figure 17. Left elevator-off case.

the false alarm rate was 0. The good performance recorded for Self #2 is due to the fact that it includes information about pilot input and a measure of the difference between normal and abnormal aircraft response. The higher dimensional Self #3, which includes the features of Self #1 and #2, performs better, as expected. However, considering Self #1 and #2 individually but combined within the detection logic produces even better detection results. This confirms the hypothesis behind the hierarchical multi-self strategy, which states that lower dimensional projections, if properly combined, may produce as good detection performance as higher dimensional single selves while avoiding associated computational issues[11]. Finally, the best results are obtained using a combination of the three selves.

https://doi.org/10.1017/S0001924000009532 Published online by Cambridge University Press

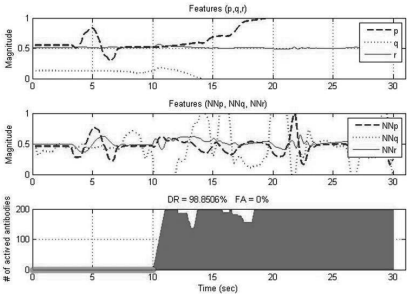


Figure 18. Left stabiliser-off case.

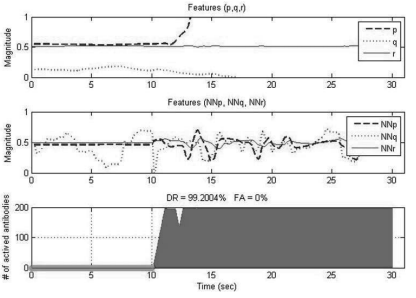


Figure 19. Jam of left elevator case.

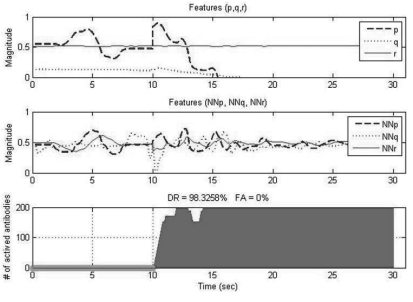


Figure 20. Jam of right elevator case.

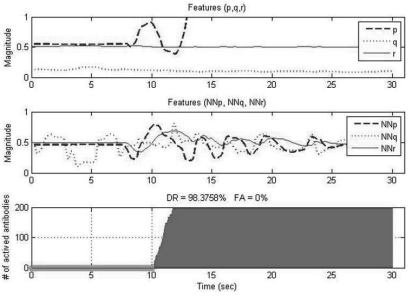


Figure 21. Jam of left aileron case.

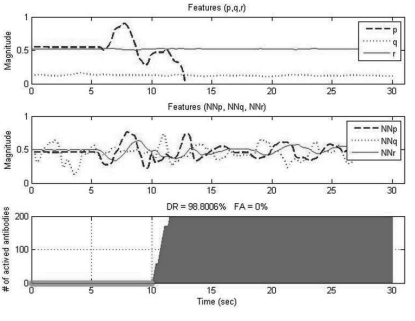


Figure 22. Jam of right aileron case.

Figures 12 through 22 display detection results for different fault detection scenarios using the combination of the three selves. In all the figures, the top two subplots show the normalised data for all the features used to build the selves outlined in Table 3 (p, q, r, NNp, NNq and NNr). The bottom subplot shows the number of antibodies (or detectors) that detected failure over a previous one-second window. When the plot shows a zero value, then no abnormal condition is detected, while a non-zero value means exactly the opposite. The highest value of activated antibodies is always 200 since the sampling rate used in the detection scheme was 200Hz. All types of faults occur at 10 sec, and in all of the cases the anomaly alarm is triggered at this time as reflected in each of the detection result figures. The flight test for validation of the AIS at nominal conditions

https://doi.org/10.1017/S0001924000009532 Published online by Cambridge University Press

Table 5
Identification performance of the AIS-based FDI scheme

Identified failure → Actual failure ↓	Rudder off	Vertical tail off	Left outboard flap off	Left wingtip off	Left elevator off	Left stabiliser off	Left elevator jam	Right elevator jam	Left aileron jam	Right aileron jam
Rudder off	**100**	0	0	0	0	0	0	0	0	0
Vertical tail off	0	**100**	0	0	0	0	0	0	0	0
Left outboard flap off	0	0	**98·58**	1·42	0	0	0	0	0	0
Left wingtip off	0	0	6·58	**90·84**	0	0	0	0	0	2·58
Left elevator off	0	0	0	0	**96·61**	0	0	0	0	3·39
Left stabiliser off	0	0	0	0	0	**99·91**	0	0	0·09	0
Left elevator jam	0	0	0	0	0	0	**100**	0	0	0
Right elevator jam	0	0	0	0	0	0·02	0·02	**99·96**	0	0
Left aileron jam	0	0·62	0	0	0	0	0·02	0	**99·36**	0
Right aileron jam	0	0·35	3·30	1·70	0	0	0	0·05	0	**94·60**

were normalised and used to test the antibodies as shown in Fig. 12. With false alarms of 0%, the validation results at nominal conditions are considered excellent.

Once a failure condition has been declared by the detection phase, the identification phase of the AIS- based FDI scheme starts to attempt a classification according to the category/type of failure (Table 2). In this example, an FDI scheme configuration using self #3 was used. As described in Section 4.0 and Fig. 4, detectors have been labeled as identifiers to correspond to one of the ten failure categories. The failure category is determined based on the number of times each set of identifiers is activated. The most repetitive outcome determines the identified category. The identification rates presented in Table 5 are computed with respect to the number of points for which detection was successful. The rows of Table 5 correspond to the actual failure and the columns, to the outcome of the identification phase. For example, a failure consisting of the total destruction of the left outboard flap was identified correctly in 98·58% of cases and it was identified as a destruction of the left wing tip in 1·42% of cases.

These results show that the AIS- based FDI scheme provides an excellent performance for both the failure detection and identification phases for all cases considered.

8.0 CONCLUSIONS

A neurally-augmented AIS has been proposed in this paper for aircraft sub-system failure detection and identification. The neural estimation of angular accelerations, as part of the AIS feature set, proved to possess excellent FDI capabilities for the types of abnormal conditions investigated. The proposed approach allows for the development of generic aircraft-independent FDI schemes.

https://doi.org/10.1017/S0001924000009532 Published online by Cambridge University Press

The WVU computational environment for AIS design and testing was used to develop and demonstrate the proposed integrated FDI scheme for the NASA GTM. Despite the complexity of the process, the WVU computational tools allow for an efficient, streamlined design.

The proposed FDI scheme achieves excellent performance in terms of false alarms and detection rates over wide areas of the flight envelope for several types of actuator and aerodynamic surface failures and damages.

The capability of the hierarchical multi-self strategy to produce high detection performance while using lower dimensional projections of the self was confirmed.

The potential of the AIS paradigm to address directly the complexity and multi-dimensionality of aircraft dynamic response in the context of integrated abnormal condition detection and identification and its capability to provide adequate tools for a comprehensive solution to this problem have been confirmed.

ACKNOWLEDGEMENT

This work has been supported in part by NASA under Co-operative Agreement no. NNX08AC60A, by the NASA West Virginia Space Grant Consortium through a grant within the Graduate Research Fellowship Program, and by the Army Research Laboratory under Co-operative Agreement no. W911NF-10-2-0110.

REFERENCES

1. 2011 NASA Strategic Plan, 2011, National Aeronautics and Space Administration, http://www.nasa.gov/pdf/516579main_NASA2011StrategicPlan.pdf
2. National Aeronautics Research and Development Policy, February 2010, Executive Office of the President of the United States, National Science and Technology Council, http://www.whitehouse.gov/sites/default/files/microsites/ostp/aero-rdplan-2010.pdf
3. ABBOTT, D. *et al*. Concepts for an integrated vehicle health monitoring system, *Review of Progress in QNDE*, 2003, **22**, AIP Conference Proceedings.
4. FUDGE, M., STAGLIANO, T. and TSIAO, S. Non-Traditional Flight Safety Systems & Integrated Vehicle Health Management Systems — Descriptions of Proposed & Existing Systems and Enabling Technologies & Verification Methods, Final Report, 2003, The Office of the Associate Administrator for Commercial Space Transportation, Federal Aviation Administration.
5. BELCASTRO, C.M. and JACOBSON, S.R. Future integrated systems concept for preventing aircraft loss-of–control accidents, 2010, PAIAA Guidance, Navigation, and Control Conference, August 2010, Toronto, Canada.
6. TOTAH, J., KRISHNAKUMAR, K. and VIKEN, S. Integrated Resilient Aircraft Control — Stability, Maneuverability, and Safe Landing in the Presence of Adverse Conditions, April 2007, Project Technical Plan, NASA.
7. KRISHNAKUMAR, K. Artificial Immune System Approaches for Aerospace Applications, 2003, AIAA-2003-0457, 41st Aerospace Sciences Meeting & Exhibition, Reno, NV, USA.
8. DASGUPTA, D., KRISHNAKUMAR, K., WONG, D. and BERRY, M. Negative selection algorithm for aircraft fault detection, 2004, NICOSIA, G. *et al* (Eds), ICARIS 2004, LNCS 3239, pp 1-13.
9. PERHINSCHI, M.G., MONCAYO, H. and DAVIS, J. Integrated framework for artificial immunity-based aircraft failure detection, identification, and evaluation, *AIAA J Aircr*, Nov-Dec 2010, **47**, (6), pp 1847-1859.
10. PERHINSCHI, M.G., MONCAYO, H. and AL AZZAWI, D. Development of immunity-based framework for aircraft abnormal conditions detection, identification, evaluation and accommodation, 2013, AIAA Guidance, Navigation, and Control Conference, August 2013, Boston, MA, USA.
11. MONCAYO, H., PERHINSCHI, M.G. and DAVIS, J. Aircraft failure detection and identification using an immunological hierarchical multi-self strategy, *AIAA J Guidance, Control and Dynamics*, July-Aug 2010, **33**, (4), pp 302-320.

https://doi.org/10.1017/S0001924000009532 Published online by Cambridge University Press

12. MONCAYO, H., PERHINSCHI, M.G. and DAVIS, J. Artificial immune system – based aircraft failure detection and identification over an extended flight envelope, *Aeronaut J*, Jan 2011, **115**, (1163).
13. MONCAYO, H. and PERHINSCHI, M.G. *Aircraft Fault Tolerance: A Biologically Inspired Immune Framework for Sub-System Failures*, 2011, VDM Verlag Dr Muller GmbH & Co KG, VDM Publishing House Ltd, Saarbruecken, Germany.
14. DAVIS, J., PERHINSCHI, M.G. and MONCAYO, H. Evolutionary algorithm for artificial immune system-based failure detector generation and optimization, *AIAA J Guidance, Control and Dynamics*, **33**, (2), pp 302-320, Mar-Apr 2010.
15. MONCAYO, H., PERHINSCHI, M.G. and DAVIS, J. Simulation environment for the Development and Testing of Immunity-Based Aircraft Failure Detection schemes, Proceedings of the AIAA Modeling and Simulation Technologies Conference, August 2011, Portland, OR, USA.
16. PERHINSCHI, M.G., MONCAYO, H., WILBURN, B., BARTLETT, A., DAVIS, J. and KARAS, O. Testing of immunity-Based failure detection scheme with the NASA Generic Transport Model, 2011, AIAA Guidance, Navigation, and Control Conference, August 2011, Portland, OR, USA.
17. JORDAN, T.L., FOSTER, J.V., BAILEY, R.M. and BELCASTRO, C.M. AirSTAR: A UAV platform for flight dynamics and control system testing, 2006, AIAA 2006-3307, 25th AIAA Aerodynamic Measurement Technology and Ground Testing Conference, San Francisco, CA, USA.
18. JORDAN, T.L., LANGFORD, W.M. and HILL, J.S. Airborne subscale transport aircraft research testbed: aircraft model development, 2005, AIAA Guidance, Navigation, and Control Conference and Exhibit, 15-18 August 2005, San Francisco, CA, USA.
19. BENJAMINI, E. *Immunology, A Short Course*, 1992, Wiley-Liss Publications, New York, NY, USA.
20. FARMER, J., NORMAN, H., PACKARD, S. and PERELSON, A.S. The Immune System, Adaptation, and Machine Learning, *Physica*, 1986, **22D**, pp 187-204, North-Holland, Amsterdam, The Netherlands.
21. FORREST, S, PERELSON, A.S., ALLEN, L. and CHERUKURI, R. Self-nonself discrimination in a computer,1994, IEEE Symposium on Research in Security and Privacy, pp 202-212, IEEE Computer Society Press, Los Alamitos, CA, USA.
22. DASGUPTA, D. and ATTOH-OKINE, N. Immunity-based systems: a survey, 1997, IEEE International Conference on Systems, Man and Cybernetics, Orlando, FL, USA.
23. MONCAYO, H. Immunity-based detection, identification, and evaluation of aircraft sub-system failures, 2009, PhD Dissertation, Dept of Mechanical and Aerospace Engineering, West Virginia University, USA.
24. DAVIS, J. The Design of an Evolutionary Algorithm for Artificial Immune System Based Failure Detector Generation and Optimization, 2010, MSc thesis, Dept of Mechanical and Aerospace Engineering, West Virginia University, USA.
25. BELCASTRO, C.M. and FOSTER, J.V. Aircraft loss-of-control accident analysis, 2010, AIAA Guidance, Navigation, and Control Conference, August 2010, Toronto, Canada.
26. PERHINSCHI, M.G., MONCAYO, H., DAVIS, J., WILBURN, B., KARAS, K. and WATHEN M. Development of a simulation environment for autonomous flight control algorithms, 2011, AIAA Modeling and Simulation Technologies Conference, August 2011, Portland, Oregon, USA.
27. PERHINSCHI, M.G., WILBURN, B., WILBURN, J., MONCAYO, H. and KARAS, O. Simulation environment for UAV fault tolerant Autonomous Control Laws Development, *J Modeling, Simulation, Identification, and Control*, 2013, 1, (4), pp 164-195.
28. The FlightGear Manual, August 2011, http://mapserver.flightgear.org/getstart/
29. LU, Y., SUNDARARAJAN, N. and SARATCHANDRAN, P. Analysis of minimal radial basis function network algorithm for real time identification of nonlinear dynamic systems, *IEEE Proceedings on Control Theory and Application*, 2000, **4**, (147), p 476.

https://doi.org/10.1017/S0001924000009532 Published online by Cambridge University Press